




# Nanoscale phase separation on an AlGaIn surface characterized by scanning diffusion microscopy

BOYANG LIU,<sup>1,2</sup>  ZHENGHUI LIU,<sup>1,2,4</sup> GENGZHAO XU,<sup>1,2</sup> WENTAO SONG,<sup>1,2</sup> CHUNYU ZHANG,<sup>1,2</sup> KEBEI CHEN,<sup>1,2</sup> SHA HAN,<sup>1,2</sup> XIAOJUAN SUN,<sup>3,5</sup> DABING LI,<sup>3</sup> AND KE XU<sup>1,2,6</sup>

<sup>1</sup>School of Nano-Tech and Nano-Bionics, University of Science and Technology of China, No. 96, JinZhai Road Baohe District, Hefei, Anhui 230026, China

<sup>2</sup>Suzhou Institute of Nano-Tech and Nano-Bionics, Chinese Academy of Sciences, Suzhou 215123, China

<sup>3</sup>Changchun Institute of Optics, Fine Mechanics and Physics, Chinese Academy of Sciences, Changchun 130033, China

<sup>4</sup>zhliu2007@sinano.ac.cn

<sup>5</sup>sunxj@ciomp.ac.cn

<sup>6</sup>kxu2006@sinano.ac.cn

**Abstract:** AlGaIn is an important material for deep ultraviolet optoelectronic devices and electronic devices. The phase separation on the AlGaIn surface means small-scale compositional fluctuations of Al, which is prone to degrade the performance of devices. In order to study the mechanism of the surface phase separation, the Al<sub>0.3</sub>Ga<sub>0.7</sub>In wafer was investigated by the scanning diffusion microscopy method based on the photo-assisted Kelvin force probe microscope. The response of the surface photovoltage near the bandgap was quite different for the edge and the center of the island on the AlGaIn surface. We utilize the theoretical model of scanning diffusion microscopy to fit the local absorption coefficients from the measured surface photovoltage spectrum. During the fitting process, we introduce *as* and *ab* parameters (bandgap shift and broadening) to describe the local variation of absorption coefficients  $\alpha(as, ab, \lambda)$ . The local bandgap and Al composition can be calculated quantitatively from the absorption coefficients. The results show that there is lower bandgap (about 305 nm) and lower Al composition (about 0.31) at the edge of the island, compared with those at the center of the island (about 300 nm for bandgap and 0.34 for Al composition). Similar to the edge of the island, there is a lower bandgap at the V-pit defect which is about 306 nm corresponding to the Al composition of about 0.30. These results mean Ga enrichment both at the edge of the island and the V-pit defect position. It proves that scanning diffusion microscopy is an effective method to review the micro-mechanism of AlGaIn phase separation.

© 2023 Optica Publishing Group under the terms of the [Optica Open Access Publishing Agreement](#)

## 1. Introduction

AlGaIn is a direct bandgap semiconductor material. The bandgap of AlGaIn changes when the Al components increasing from 3.42 eV to 6.20 eV. In recent years, AlGaIn materials have been widely used in the field of solid-state deep ultraviolet photoelectric devices, including deep ultraviolet light-emitting diodes (LED), lasers, and photodetectors [1–3]. AlGaIn is also an important material for electronic power devices such as high electron mobility transistors (HEMT) and Schottky diodes with high breakdown voltage [4–8]. The performance of these devices depends on the crystal quality of the AlGaIn material. Especially for the AlGaIn materials with high Aluminum composition, the surface migration velocity of Al and Ga atoms vary greatly during the epitaxy growth process, which leads to small-scale phase separation [9–11]. This may increase the density of local states, and affect the carrier transport and the light emission process,

thus degrading the luminescent performance [12,13]. To improve the device's performance, researchers have explored how to effectively suppress phase separation by adjusting the stress during the growth process [14]. In the field of test analysis, various methods are used to study the micro-mechanism for phase separation to support the improvement of the epitaxy process, such as photoluminescence spectrum (PL), cathodoluminescence spectrum (CL), and near-field scanning optical microscopy (SNOM). One of the main characteristics of phase separation is that there are multiple emission peaks in the photoluminescence spectrum. The spatial resolution of the commonly applied confocal photoluminescence spectrum is at the micron-scale, reflecting the spectral changes around larger V-pits and defect structures over  $10\text{ }\mu\text{m}$ , corresponding to the component heterogeneity. For smaller structures, it can be measured by cathodoluminescence spectroscopy [15,16] and SNOM [10,17–19] methods with a resolution of  $100\text{ nm}$ . For example, A. Knauer et al. [15] used the CL method to find the deviation of the luminescence peak at the edge of the step due to the phase separation. Andrea Pinos [10,18] et al. used the SNOM method to find the deviation of the near-field fluorescence spectrum peak at the edge of the island structure on the AlGaIn surface, which corresponds to the enrichment of Ga near the step. All these characterization methods are based on luminescence peaks. However, for non-recombination centers such as V-pit defects, the luminescence spectrum is hard to acquire and analyzed.

In this paper, we demonstrate a realization of scanning diffusion microscopy method [20] to explore the nanoscale phase separation on the AlGaIn surface. The method is based on photo-assisted Kelvin-probe force microscope (KPFM) which can acquire surface photovoltage (SPV) with nanoscale spatial resolution at different light wavelength  $\lambda$ . The responses of surface photovoltage near the bandgap are quite different for the center and the edge of the island structures. By fitting the surface photovoltage curve  $SPV(\lambda)$ , the local absorption coefficient spectrum are calculated. The different values of bandgap  $E_g$  and Al composition  $x$  at the center and the edge of the island structures are quantitatively calculated from the local absorption coefficient spectrum. The results show that the value of  $E_g$  at the island edge is lower than that at the island center. These results are consistent with the description that the Ga-rich regions are around island boundaries and layer steps in the previous references. Similar to the edge of the island, there is also a lower bandgap and lower Al composition at the V-pit defect. It proves that the scanning diffusion microscopy method based on photo-assisted Kelvin-probe force microscope is an effective method to review the nanoscale mechanism of AlGaIn phase separation.

## 2. Experiments and methods

The sample is an  $\text{Al}_{0.3}\text{Ga}_{0.7}\text{N}$  wafer with nominal Al ratio of about 0.3. AlGaIn epitaxial layers are grown on sapphire substrates with AlN templates by metal organic chemical vapor deposition (MOCVD). A scanning electron microscope (SEM, S-4800 of HITACHI Company, Japan) was applied to scan the fresh cleaved cross section of the sample. The SEM image is shown in Fig. 1(a), in which the thickness of the AlGaIn layer and AlN layer is marked.

The photoluminescence (PL) spectrum was obtained by our home-built deep UV confocal time-resolved photoluminescence spectrum system. The excitation light source is a  $266\text{ nm}$  femtosecond pulsed laser with an average power of about  $1\text{ mW}$ . The laser is focused to the sample surface through a reflective objective lens. The excited photoluminescence is collected through the same objective lens and then focused to a pinhole, which is then received by the spectrometer to obtain a confocal photoluminescence spectrum. The spatial resolution of the PL spectrum is about  $2\text{ }\mu\text{m}$ . The typical PL result and the peak separation fitting results are shown in Fig. 1(b). There is one peak at  $300.5\text{ nm}$  and one peak at  $306.6\text{ nm}$ , which represents two different bandgaps, indicating that the  $\text{Al}_{0.3}\text{Ga}_{0.7}\text{N}$  wafer has phase separation.

The surface photovoltage spectrum was acquired by a home-built photo-assisted KPFM system with the schematics described in our previously published paper [20,21]. Different from the

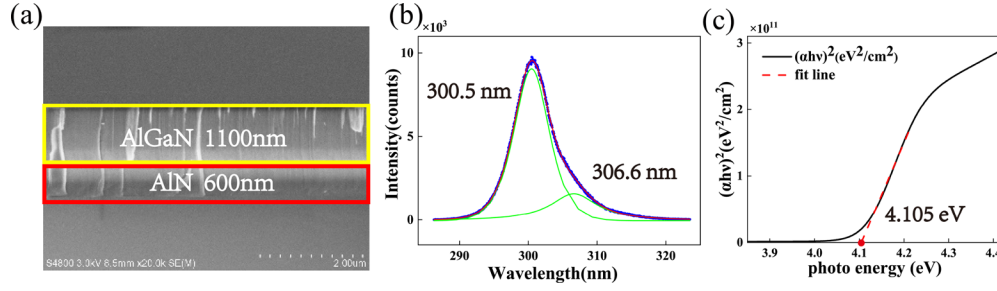


**Fig. 1.** (a) SEM image of the cross-section of the  $\text{Al}_{0.3}\text{Ga}_{0.7}\text{N}$  sample, in which the thickness of the AlGaIn layer and AlN layer are marked; (b) typical photoluminescence spectrum of  $\text{Al}_{0.3}\text{Ga}_{0.7}\text{N}$  sample; (c) using the measured absorption coefficients to fit the bandgap of  $\text{Al}_{0.3}\text{Ga}_{0.7}\text{N}$ .

commonly used two-pass mode, the KPFM measurement is performed in single-pass mode on an atomic force microscope (NTEGRA SPECTRA, NT-MDT) with details described in our previously published paper [20]. Applying this mode, the topography and the surface potential can be measured simultaneously in a single-pass scan and the spatial resolution of the surface potential is about 10 nm. The typical resonance frequencies  $\omega_1$  and  $\omega_2$  of the tips (ACCESS-EFM, Appnano) are about 67 kHz and 420 kHz, respectively. The tunable monochromatic light focused on the tip apex during the  $\text{SPV}(\lambda)$  measurement is generated by a white light source (Laser-Driven Light Source, EQ99, Energetiq) and a monochromator (IHR320, Horiba JY). In our experiments, the slit width of the monochromator is 0.5 mm corresponding to about 2 nm spectral resolution. The light spot diameter ( $D_{\text{flux}}$ ) on the sample is about 22.5  $\mu\text{m}$  and the light power ( $P_w$ ) is measured by the power meter to calculate the light flux  $P_0(\lambda)$  [20].

The  $\text{SPV}(\lambda)$  measurement is performed by ramping the light wavelength from 345 nm - 280 nm with a fixed step of 0.4 nm. A shutter is installed on the path of the incident light. For each wavelength  $\lambda$ , the shutter is closed and the scan will be performed in KPFM mode and the surface potential values in darkness are recorded as  $V_{\text{dark}}(\lambda)$ . Then the shutter is opened to illuminate the sample. The tip is held until a steady surface potential is measured. Then the topography and the surface potential values are scanned and recorded as  $V_{\text{light}}(\lambda)$ . At each pixel, the SPV spectrum  $\text{SPV}(\lambda) = V_{\text{light}}(\lambda) - V_{\text{dark}}(\lambda)$  is calculated.

The initial absorption coefficients  $\alpha(\lambda)$  of the AlGaIn sample is measured by a variable angle spectroscopic ellipsometer (VASE, M2000DI manufactured by J. A. Woollam Co.Inc.). The complex dielectric functions are fitted at each wavelength. A PSEMI model [22] is applied to fit the dielectric functions. The absorption coefficients can be calculated from the dielectric functions with the PSEMI model and the fitted 11 parameters:  $\alpha(\lambda) = \text{PSEMI}(E_n, B_r, \dots, \lambda)$ , where  $E_n$  is the absorption edge offset and  $B_r$  is the absorption edge broaden. A typical absorption coefficient curve near the bandgap of the AlGaIn sample is shown in Fig. 1(c).

During the fitting process of  $\text{SPV}(\lambda)$ , we introduce  $as$  and  $ab$  parameters to describe the local variation of absorption coefficients  $\alpha(as, ab, \lambda)$ . For  $as = 0$  and  $ab = 1$ , the  $\alpha(as = 0, ab = 1, \lambda)$  presents the initial absorption coefficients. For  $as \neq 0$ , the absorption edges will have a blue or red shift which means the shift of the bandgap. For  $ab \neq 1$ , the absorption edges will be steeper or broadened. Then the local absorption coefficients can be described with following equation [20]:

$$\alpha(as, ab, \lambda) = \text{PSEMI}(E_n + as, B_r \times ab, \dots, \lambda) \quad (1)$$

The local variation of absorption coefficients can be ascribed to local environmental perturbations including the small-scale composition fluctuations of Al.

Finally, The following equation is applied to fit the bandgap shift  $as$ , the bandgap broadening  $ab$ , minority carrier diffusion length  $L$ , and the parameter  $R_0$  related to the rate of surface recombination from  $SPV(\lambda)$  [20]:

$$\left( e^{q \times SPV(\lambda) / (k_0 T)} - 1 \right) / P_0(\lambda) = \left( 1 - e^{\alpha(as, ab, \lambda) \times L} \right) / R_0 \quad (2)$$

where  $q$  is the electron charge,  $k_0$  is the Boltzmann constant,  $T$  is the temperature,  $P_0(\lambda)$  is the incoming light flux,  $R_0$  is a parameter related to the surface recombination velocity. The details of the theoretical model are presented in our previous published literatures [20,21].

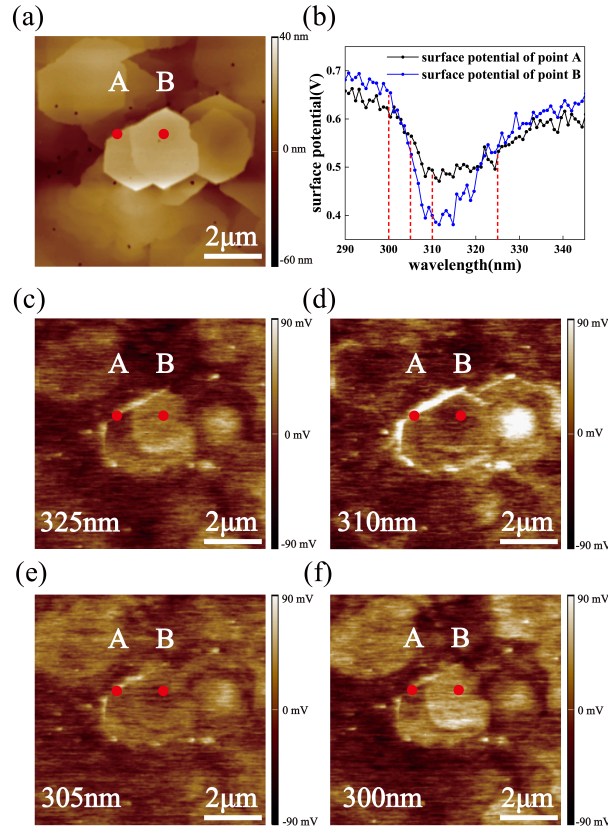
### 3. Results and discussions

Figure 2(a) shows the surface morphology of the  $\text{Al}_{0.3}\text{Ga}_{0.7}\text{N}$  sample with the size of  $20\ \mu\text{m}$ . The surface of the sample in this area is composed of several micron scale island mesas. The marked positions A and B are at the edge and the center of an island, respectively. Figure 2(b) shows the surface potential measured at positions A and B. Figures 2(c)–(f) show the surface potential distribution illuminated with light wavelength at 325 nm, 310 nm, 305 nm, and 300 nm, respectively. In order to clearly compare the surface potential contrast changes of different position, all the above surface potential images are 0th order flattened with the same data scale of  $\pm 90\ \text{mV}$ . As shown in Fig. 2(b), there is a drop of the surface potential in the wavelength range from 345 nm towards 325 nm for both position A and B. Such a drop can be explained by the absorption of light near the interface between the AlGa $\text{N}$  layer and the AlN buffer layer. The light-generated holes diffused to the interface while the electrons diffused to the surface of the AlGa $\text{N}$  [23,24]. The collection of electrons at the surface lowers the surface potential for both positions. As shown in Fig. 2(c), under 325 nm illumination which is lower than the AlGa $\text{N}$  bandgap (about 302 nm, from Fig. 1(c)), the surface potential at the edge (position A) is a little higher than that at the center (position B) of the island. Then as shown in Fig. 2(b) in the range from 325 nm towards 310 nm, the potential drop at the edge of the island is much lower than that at the center. Such a result means more and more absorption of light and holes collected at the edge of the island while little absorption occurs at the center. So under 310 nm illumination, as shown in Fig. 2(d), the surface potential at the edge is much higher than that at the center and the potential contrast between positions A and B reaches the largest. Then in the wavelength range from 310 nm to 305 nm, as shown in Fig. 2(b), the potential at the center begin to rise quickly corresponding to high light absorption. Finally, under 300 nm illumination which is higher than the AlGa $\text{N}$  bandgap, the potential contrast between position A and B reversed. The potential at the center exceeds that at the edge, as shown in Fig. 2(f). The surface potential spectrum and these potential images clearly show the different absorption coefficients between the edge (position A) and the center (position B) of the island.

When the wavelength of the incident light is lower than the bandgap, the photon energy is insufficient to cause electron transition, resulting in weak light absorption. Conversely, when the wavelength of the incident light is higher than the bandgap, the valence band electrons absorb energy and transition to the conduction band, leading to a sharp increase in light absorption. Therefore, there is a significant difference in carrier diffusion before and after the bandgap, resulting in different surface potential distributions. The surface potential changes at the edge and center of the islands in Fig. 2 under monochromatic light at wavelengths of 325 nm, 310 nm, 305 nm, and 300 nm fully demonstrate that the bandgap of point A at the edge of the islands is between 310 nm and 305 nm, while the bandgap of point B inside the islands is between 305 nm and 300 nm, which is highly consistent with the emission peak positions in the PL spectrum.

In order to quantitatively study the local absorption coefficients change of AlGa $\text{N}$ , we fitted the  $SPV(\lambda)$  spectrum following Eq. (2) in the range from 325 nm to 287 nm pixel by pixel on the line through positions A, B and C as shown in Fig. 3(a). Figure 3(b) shows a typical fitting





**Fig. 2.** (a) Surface topography image of Al<sub>0.3</sub>Ga<sub>0.7</sub>N; (b) surface potential change of point A and point B; (c)–(f) are the surface potential images under the monochromatic light of 325 nm, 310 nm, 305 nm, and 300 nm.

process with the left and right parts of Eq. (2) and the fitted local absorption coefficients plotted. Figure 3(c) shows the surface topography profile on line ABC. Figure 3(d) shows the surface potential profile under the irradiation of 310 nm monochromatic light. As shown in Fig. 3(e), the bandgap  $E_g$  was calculated from the fitted local absorption coefficients  $\alpha(as, ab, \lambda)$ . There is lower bandgap (about 305 nm) at the edge of the island (position A and C), compared with those at the center of the island (about 300 nm at position B).

In previous published work on GaN surface, The variation of the bandgap  $E_g$  at nanoscale was ascribed to several reasons [20]: (1) the local environmental perturbations including the local tilted potential near the surface in the depletion region corresponds to a bandgap shift of about 2 meV to 6 meV; (2) the spectrum resolution of the light sources applied in the ellipsometer and the photo-assisted KPFM setups. The typical spectrum resolution of 1.6 nm for our ellipsometer corresponds to a bandgap shift of about 15 meV. However, in this case on AlGaIn surface, the bandgap shift of different locations is as high as 5 nm (67 meV). Furthermore, the local bandgap fluctuation is consistent with the typical PL peaks (about 301 nm and 307 nm) shown in Fig. 1(b). So the local variation of absorption coefficients on AlGaIn surface should be mainly ascribed to the small-scale compositional fluctuations of Al.

As shown in Fig. 3(f), the local Al composition  $x$  is calculated from the bandgap  $E_g$  with the following equation:

$$E_g = xE_{AlN} + (1 - x)E_{GaIn} - bx(1 - x) \quad (3)$$

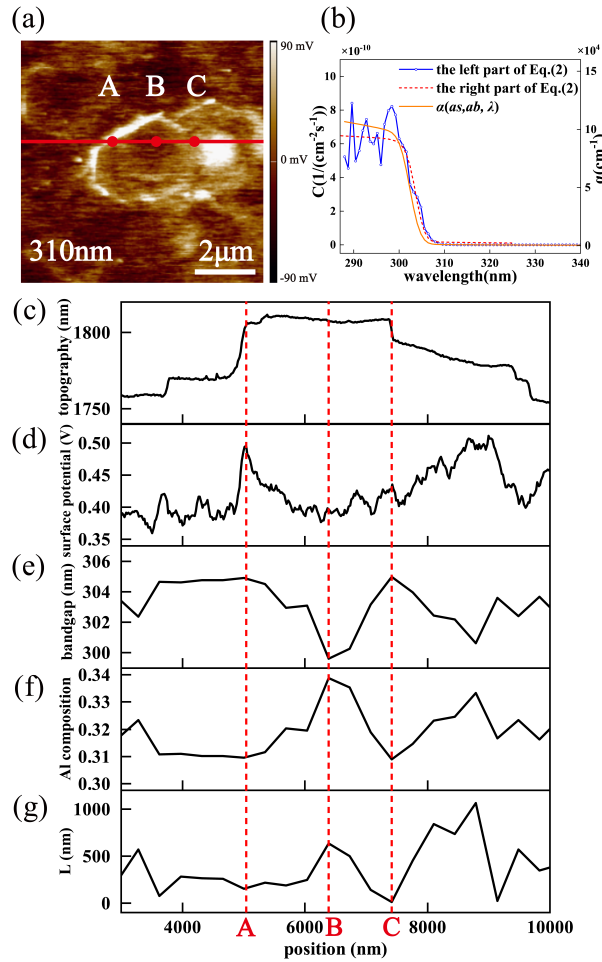


**Fig. 3.** (a) Surface potential image of  $\text{Al}_{0.3}\text{Ga}_{0.7}\text{N}$  irradiated by 310 nm monochromatic light; (b) typical fitting process of Eq. (2). The blue line is the curve calculated from the experimental data according to the left side of Eq. (2), and the red dotted line is the curve fitted according to the right side of Eq. (2). The orange solid line is the absorption coefficient corrected by parameter  $as$  and  $ab$ . (c) The surface topography profile on line ABC; (d) surface potential profile on line ABC under the irradiation of 310 nm monochromatic light; (e) bandgap variation on line ABC calculated from the fitted local absorption coefficients. (f) Al composition variation on line ABC; (g) fitted minority carrier diffusion length  $L$  on line ABC.

where  $E_{\text{AlN}}$  is the bandgap of AlN ( $\approx 6.20 \text{ eV}$ );  $E_{\text{GaN}}$  is the bandgap of GaN ( $\approx 3.42 \text{ eV}$ ) [25]; and  $b$  ( $\approx 1 \text{ eV}$ ) is the bowing parameter [26]. There is lower Al composition (about 0.31) at the edge of the island (position A and C), compared with those at the center of the island (about 0.34 at position B). These results mean a Ga enrichment at the edge of the island which makes the local bandgap lower.

The structure of the  $\text{Al}_{0.3}\text{Ga}_{0.7}\text{N}$  sample used in this paper is sapphire / AlN / AlGaIn. During the epitaxy process of the AlGaIn layer, the Ga atom had a larger migration rate and a longer migration distance than the Al atom at the same temperature. At the substrate surface with macro-steps, Ga atoms reach the boundary of the islands more quickly than Al atoms, while Al

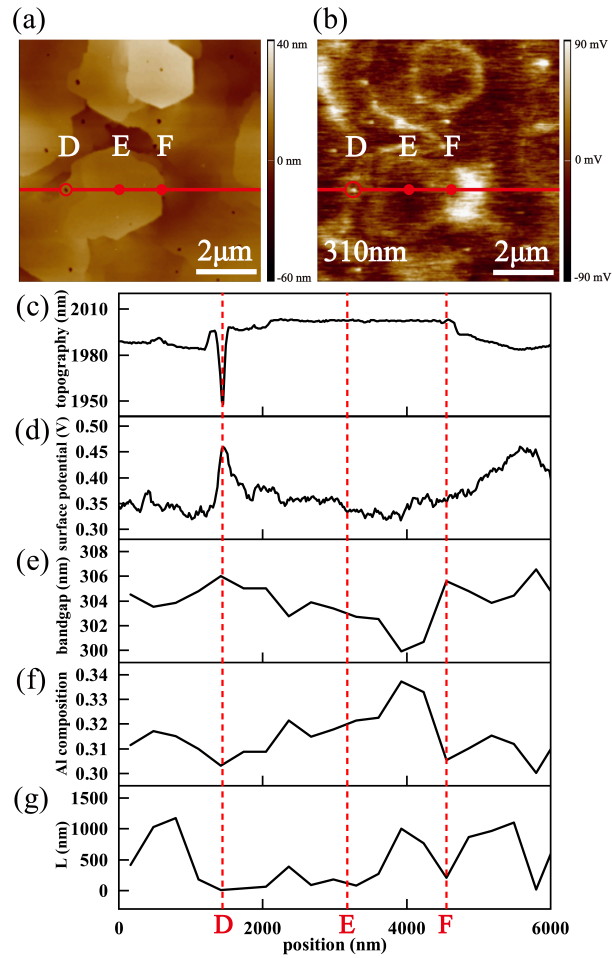


**Fig. 4.** (a) Surface topography image of  $\text{Al}_{0.3}\text{Ga}_{0.7}\text{N}$  sample; (b) surface potential image of  $\text{Al}_{0.3}\text{Ga}_{0.7}\text{N}$  irradiated by 310 nm monochromatic light; (c) surface topography profile on line DEF; (d) surface potential profile on line DEF under the irradiation of 310 nm monochromatic light; (e) bandgap variation on line DEF calculated from the fitted local absorption coefficients; (f) Al composition variation on line DEF; (g) fitted minority carrier diffusion lengths on line DEF.

atoms cannot have the same distribution with Ga atoms [9,10,13]. This resulted in the enrichment of Ga atoms at the edge of the islands [10,11,27]. The experimental results of this paper agree with the conclusions of previous references. As there are more Ga atoms at the edge of the islands compared to the inside, according to Vegard's law (Eq. (3)), the bandgap of the edge correspond to a longer wavelength, leading to different emission peaks in the PL spectrum. Moreover, the different bandgap results in varying local absorption coefficients between the edge and the interior of the islands, which generates different surface potential distributions at these positions under illumination of monochromatic light at different wavelengths.

As shown in Fig. 3(g), the fitted minority carrier diffusion length  $L$  on line ABC was also calculated by fitting Eq. (2). The minority carrier diffusion length of point B (633 nm) in the island region is larger than those of point A (150 nm) and C (15 nm) at the edges, due to the

presence of numerous dislocations and defects at the edges that hinder the long-range diffusion of minority carriers.

The change of the local absorption coefficient can also be found at some V-pit defects on the surface. Figure 4(a) is the surface topography image of another region on the  $\text{Al}_{0.3}\text{Ga}_{0.7}\text{N}$  surface and Fig. 4(c) shows the surface topography profile on the line DEF. There is a V-pit at position D. Position E and F are at the center and the edge of the island, respectively. Figure 4(b) is the surface potential distribution of this region under the irradiation of 310 nm monochromatic light and Fig. 4(d) shows the surface potential profile on the line DEF. Similar to the absorption behavior shown in Fig. 2, both positions D and F have larger potential than position E under irradiation of light with a wavelength little lower than the bandgap of the sample. The  $SPV(\lambda)$  spectrum was fitted following Eq. (2). The bandgap  $E_g$  and Al composition were calculated and shown in Fig. 4(e) and Fig. 4(f), respectively. There is a lower bandgap (about 306 nm) and lower Al composition (about 0.30) at the V-pit defect (position D), compared with those at the center of the island (about 303 nm for bandgap and 0.32 for Al composition at position E). The results present that the V-pit defects can be one of the origins of phase separation on the AlGaIn surface. As shown in Fig. 4(g), the minority carrier diffusion length at point D (10 nm) where V-pits are located is also smaller than that of point E (130 nm) inside the island, which is also attributed to the hindering effect of V-pits on the long-range diffusion of minority carriers.

#### 4. Conclusions

We applied a realization of scanning diffusion microscopy method based on the photo-assisted Kelvin-probe force microscope to explore the nanoscale mechanism of the phase separation of AlGaIn. The theoretical model presents not only minority diffusion lengths but also local absorption coefficients by fitting the surface photovoltage spectrum  $SPV(\lambda)$ . The local bandgap  $E_g$  and Al composition  $x$  can be calculated from the fitted absorption coefficients with nanoscale spatial resolution. The response of the surface photovoltage near the bandgap was quite different for the edge and the center of the island on the AlGaIn surface. The bandgap at the edge of the island is about 305 nm corresponding to the Al composition of about 0.31, while the bandgap inside the island is about 300 nm corresponding to the Al composition of about 0.34. This is consistent with the PL spectrum results with two peaks fitted at 301 nm and 307 nm. The experimental results at the V-pits defects are similar to those at the edge of the island. Our experiments show that the edges of the islands and V-pits on AlGaIn surfaces are the main reasons for nanoscale composition fluctuations and the phase separation in the PL spectrum. Scanning diffusion microscopy is an effective method to review the phase separation on the AlGaIn surface at the nanoscale.

**Funding.** Chinese Academy of Sciences Key Technology Talent Program (Z. Liu); Chinese Academy of Sciences Pioneer Hundred Talents Program (W. Song); Fundamental Research Pilot Project of Suzhou (SJC2021007, SJC2021010); Young Scientists Fund of NSFC (12204511).

**Disclosures.** The authors declare no conflicts of interest.

**Data availability.** Data underlying the results presented in this paper are not publicly available at this time but may be obtained from the authors upon reasonable request.

#### References

1. Q. Cai, Q. Li, M. Li, Y. Tang, J. Wang, J. Xue, D. Chen, H. Lu, R. Zhang, and Y. Zheng, "Performance modulation for back-illuminated AlGaIn ultraviolet avalanche photodiodes based on multiplication scaling," *IEEE Photonics J.* **11**(1), 1–7 (2019).
2. D. Li, K. Jiang, X. Sun, and C. Guo, "AlGaIn photonics: recent advances in materials and ultraviolet devices," *Adv. Opt. Photonics* **10**(1), 43–110 (2018).
3. W. Yang, J. Li, W. Lin, S. Li, H. Chen, D. Liu, X. Yang, and J. Kang, "Control of two-dimensional growth of AlN and high Al-content AlGaIn-based MQWs for deep-UV LEDs," *AIP Adv.* **3**(5), 052103 (2013).

4. H. Q. Nguyen, T. Nguyen, P. Tanner, T. K. Nguyen, A. R. M. Faisal, J. Fastier-Wooller, T. H. Nguyen, H. P. Phan, N. T. Nguyen, and D. V. Dao, "Piezotronic effect in a normally off p-GaN/AlGaIn/GaN HEMT toward highly sensitive pressure sensor," *Appl. Phys. Lett.* **118**(24), 242104 (2021).
5. B. Ozden, C. Yang, F. Tong, M. P. Khanal, V. Mirkhani, M. H. Sk, A. C. Ahyi, and M. Park, "Depth-resolved ultra-violet spectroscopic photo current-voltage measurements for the analysis of AlGaIn/GaN high electron mobility transistor epilayer deposited on Si," *Appl. Phys. Lett.* **105**(17), 172105 (2014).
6. T. Liu, H. Watanabe, S. Nitta, J. Wang, G. Yu, Y. Ando, Y. Honda, H. Amano, A. Tanaka, and Y. Koide, "Suppression of the regrowth interface leakage current in AlGaIn/GaN HEMTs by unactivated Mg doped GaN layer," *Appl. Phys. Lett.* **118**(7), 072103 (2021).
7. J. Wang, H. Zhou, J. Zhang, Z. Liu, S. Xu, Q. Feng, J. Ning, C. Zhang, P. Ma, J. Zhang, and Y. Hao, "Demonstration of Al<sub>0.85</sub>Ga<sub>0.15</sub>N Schottky barrier diode with > 3 kV breakdown voltage and the reverse leakage currents formation mechanism analysis," *Appl. Phys. Lett.* **118**(17), 173505 (2021).
8. T. Zhang, Y. Zhang, R. Li, J. Lu, H. Su, S. Xu, K. Su, X. Duan, Y. Lv, J. Zhang, and Y. Hao, "Current transport mechanism of AlGaIn-channel Schottky barrier diode with extremely low leakage current and high blocking voltage of 2.55 kV," *Appl. Phys. Lett.* **120**(9), 092102 (2022).
9. P. Chen, S. Chua, and Z. Miao, "Phase separation in AlGaIn/GaN heterojunction grown by metalorganic chemical vapor deposition," *J. Cryst. Growth* **273**(1-2), 74–78 (2004).
10. A. Pinos, V. Liuolia, S. Marcinkevicius, J. Yang, R. Gaska, and M. Shur, "Localization potentials in AlGaIn epitaxial films studied by scanning near-field optical spectroscopy," *J. Appl. Phys.* **109**(11), 113516 (2011).
11. X. Wang, D. Zhao, D. Jiang, H. Yang, J. Liang, U. Jahn, and K. Ploog, "Al compositional inhomogeneity of AlGaIn epilayer with a high Al composition grown by metal-organic chemical vapour deposition," *J. Phys.: Condens. Matter* **19**(17), 176005 (2007).
12. I. Bryan, Z. Bryan, S. Mita, A. Rice, L. Hussey, C. Shelton, J. Tweedie, J. P. Maria, R. Collazo, and Z. Sitar, "The role of surface kinetics on composition and quality of AlGaIn," *J. Cryst. Growth* **451**, 65–71 (2016).
13. K. Jiang, X. Sun, J. Ben, Z. Shi, Y. Jia, Y. Wu, C. Kai, Y. Wang, and D. Li, "Suppressing the compositional non-uniformity of AlGaIn grown on a HVPE-AlN template with large macro-steps," *CrystEngComm* **21**(33), 4864–4873 (2019).
14. T. T. Luong, Y. T. Ho, Y. Y. Wong, S. Chang, and E. Y. Chang, "Phase separation-suppressed and strain-modulated improvement of crystalline quality of AlGaIn epitaxial layer grown by MOCVD," *Microelectron. Reliab.* **83**, 286–292 (2018).
15. A. Knauer, V. Kueller, U. Zeimer, M. Weyers, C. Reich, and M. Kneissl, "AlGaIn layer structures for deep UV emitters on laterally overgrown AlN/sapphire templates," *Phys. Status Solidi A* **210**(3), 451–454 (2013).
16. Q. Sun, H. Wang, D. Jiang, R. Jin, Y. Huang, S. Zhang, H. Yang, U. Jahn, and K. Ploog, "Spatial distribution of deep level defects in crack-free AlGaIn grown on GaN with a high-temperature AlN interlayer," *J. Appl. Phys.* **100**(12), 123101 (2006).
17. S. Marcinkevicius, R. Jain, M. Shatalov, J. Yang, M. Shur, and R. Gaska, "High spectral uniformity of AlGaIn with a high Al content evidenced by scanning near-field photoluminescence spectroscopy," *Appl. Phys. Lett.* **105**(24), 241108 (2014).
18. A. Pinos, S. Marcinkevicius, V. Liuolia, J. Yang, R. Gaska, and M. S. Shur, "Scanning near-field optical spectroscopy of AlGaIn epitaxial layers," *Phys. Status Solidi C* **9**(7), 1617–1620 (2012).
19. G. Tamulaitis, "Spatial inhomogeneity of luminescence in III-nitride compounds," *Mater. Sci.* **17**(4), 343–351 (2011).
20. Y. Wang, Z. Liu, W. Song, G. Xu, K. Chen, C. Zhang, S. Han, J. Wang, and K. Xu, "Direct measurement for nanoscale vertical carrier diffusion on semiconductor surface—An approach toward scanning diffusion microscopy," *J. Appl. Phys.* **131**(11), 115701 (2022).
21. Z. Liu, K. Xu, Y. Fan, G. Xu, Z. Huang, H. Zhong, J. Wang, and H. Yang, "Local ultra-violet surface photovoltage spectroscopy of single thread dislocations in gallium nitrides by Kelvin probe force microscopy," *Appl. Phys. Lett.* **101**(25), 252107 (2012).
22. C. M. Herzinger and B. D. Johs, "Dielectric function parametric model, and method of use," US Patent 5,796,983 (1998).
23. S. Fang, D. Wang, Y. Kang, X. Liu, Y. Luo, K. Liang, L. Li, H. Yu, H. Zhang, M. H. Memon, B. Liu, Z. Liu, and H. Sun, "Balancing the Photo-Induced Carrier Transport Behavior at Two Semiconductor Interfaces for Dual-Polarity Photodetection," *Adv. Funct. Mater.* **32**(28), 2202524 (2022).
24. R. M. Doughty, F. A. Chowdhury, Z. Mi, and F. E. Osterloh, "Surface photovoltage spectroscopy observes junctions and carrier separation in gallium nitride nanowire arrays for overall water-splitting," *J. Chem. Phys.* **153**(14), 144707 (2020).
25. K. Takeuchi, S. Adachi, and K. Ohtsuka, "Optical properties of Al<sub>x</sub>Ga<sub>1-x</sub>N alloy," *J. Appl. Phys.* **107**(2), 023306 (2010).
26. N. Nepal, J. Li, M. Nakarmi, J. Lin, and H. Jiang, "Temperature and compositional dependence of the energy band gap of AlGaIn alloys," *Appl. Phys. Lett.* **87**(24), 242104 (2005).
27. Q. Sun, Y. Huang, H. Wang, J. Chen, R. Jin, S. Zhang, H. Yang, D. Jiang, U. Jahn, and K. Ploog, "Lateral phase separation in AlGaIn grown on GaN with a high-temperature AlN interlayer," *Appl. Phys. Lett.* **87**(12), 121914 (2005).